CPHT-RR116.122018, IFT-UAM/CSIC-18-130, NORDITA 2018-125

Supplemental material for 'Universal relaxation in a holographic metallic density wave phase'

Andrea Amoretti

*Dipartimento di Fisica, Università di Genova, via Dodecaneso 33, I-16146, Genova, Italy and I.N.F.N. - Sezione di Genova and Physique Théorique et Mathématique and International Solvay Institutes Université Libre de Bruxelles, C.P. 231, 1050 Brussels, Belgium**

Daniel Areán

Instituto de Física Teórica UAM/CSIC, Calle Nicolás Cabrera 13-15, Cantoblanco, 28049 Madrid, Spain†

Blaise Goutéraux

CPHT, CNRS, Ecole polytechnique, IP Paris, F-91128 Palaiseau, France and Nordita, KTH Royal Institute of Technology and Stockholm University, Roslagstullsbacken 23, SE-106 91 Stockholm, Sweden‡

and Daniele Musso

Departamento de Física de Partículas, Universidade de Santiago de Compostela and Instituto Galego de Física de Altas Enerxías (IGFAE).§

(Dated: October 7, 2019)

WIGNER CRYSTAL HYDRODYNAMICS

We briefly recap the main features of Wigner crystal hydrodynamics, in the presence of weak explicit breaking of translations. More details can be found in [1, 2]. As translations are broken spontaneously along both spatial directions, the usual conserved densities (energy, charge, momentum) need to be coupled to two Goldstone modes, φ_i, $i = x, y$. The free energy is supplemented by terms capturing the effect of the Goldstones:

$$f = \frac{1}{2}K|q\cdot\varphi(q)|^2 + \frac{1}{2}G\left(q^2+m^2\right)|\varphi(q)|^2 = \frac{1}{2}(K+G)\left|\lambda_\parallel(q)\right|^2 + \frac{G}{2}\left|\lambda_\perp(q)\right|^2 . \tag{1}$$

K and G are the bulk and shear moduli, and characterize the stiffness of phase fluctuations around the ordered state. m is the Goldstone mass generated by the explicit breaking of translations. It is convenient to parameterize the Goldstones by their longitudinal and transverse contributions, $\lambda_\parallel = \nabla\cdot\varphi$ and $\lambda_\perp = \nabla\times\varphi$. The corresponding sources $s_{\parallel,\perp}$ are defined by requiring that $\lambda_{\parallel,\perp} = \delta f/\delta s_{\parallel,\perp}$.

To leading order in gradients and keeping only linear terms, the Goldstones obey the following 'Josephson' relations

$$\begin{aligned}\partial_t\lambda_\parallel + \Omega_\parallel\lambda_\parallel =& \nabla\cdot v + \gamma_1\nabla^2\mu + \gamma_2\nabla^2 T + \frac{\xi_\parallel}{K+G}\nabla^2 s_\parallel + \dots ,\\ \partial_t\lambda_\perp + \Omega_\perp\lambda_\perp =& \nabla\times v + \frac{\xi_\perp}{G}\nabla^2 s_\perp + \dots ,\end{aligned} \tag{2}$$

where v is the velocity, μ the chemical potential, and $\gamma_{1,2}$ and $\xi_{\parallel,\perp}$ are diffusive transport coefficients. We have introduced two Goldstone damping rates $\Omega_\perp$ and $\Omega_\parallel$. They can in principle be distinct. For instance, in the presence of dislocations, the climb motion of dislocations, $\Omega_\parallel$, is suppressed [3].

These Josephson relations are supplemented by current, heat and momentum conservation equations (energy can be traded for entropy to linear order):

$$\partial_t\rho + \nabla\cdot j = 0\,, \quad \partial_t s + \nabla\cdot(j_q/T) = 0\,, \quad \partial_t\pi^i + \nabla_j T^{ji} = -\Gamma\pi^i - Gm^2\phi_i\,, \tag{3}$$

together with the constitutive relations

$$\begin{aligned} j =& \rho v - \sigma_o\nabla\mu - \alpha_o\nabla T - \gamma_1\nabla s_\parallel + \dots ,\\ j_q/T =& sv - \alpha_o\nabla\mu - (\bar\kappa_o/T)\nabla T - \gamma_2\nabla s_\parallel + \dots ,\\ T^{ij} =& \delta^{ij}\left(p + (K+G)\nabla\cdot\varphi\right) + 2G\left[\nabla^{(i}\varphi^{j)} - \delta^{ij}\nabla\cdot\varphi\right] - \eta\left(2\nabla^{(i}v^{j)} - \delta^{ij}\nabla\cdot v\right) + \dots .\end{aligned} \tag{4}$$

The underlying conformal symmetry of the holographic setup implies that the stress-energy tensor is traceless, which sets the bulk viscosity to zero.

The hydrodynamic retarded Green's functions at nonzero frequency and wavevector are derived by following the Kadanoff-Martin procedure [4, 5]:

$$G^R_{AB}(\omega,q) = M_{AC}\left[(i\omega - M)^{-1}\right]_{CD}\chi_{DB} \tag{5}$$

where the vevs $A, B = (\delta\rho, \delta s, \pi_\parallel, \lambda_\parallel, \pi_\perp, \lambda_\perp)$ and the corresponding sources are $(\delta\mu, \delta T, v_\parallel, s_\parallel, v_\perp, s_\perp)$. M is the matrix

$$M_{AB} = \begin{pmatrix} \sigma_o q^2 & \alpha_o q^2 & i\rho q & \gamma_1 q^2 & 0 & 0 \\ \alpha_o q^2 & \frac{\bar\kappa_o}{T} q^2 & isq & \gamma_2 q^2 & 0 & 0 \\ i\rho q & isq & \eta q^2 + \chi_{\pi\pi}\Gamma & iq & 0 & 0 \\ \gamma_1 q^2 & \gamma_2 q^2 & iq & \chi_{\lambda_\parallel\lambda_\parallel}\left(q^2\xi_\parallel + \Omega_\parallel\right) & 0 & 0 \\ 0 & 0 & 0 & 0 & \eta q^2 + \chi_{\pi\pi}\Gamma & iq \\ 0 & 0 & 0 & 0 & iq & \chi_{\lambda_\perp\lambda_\perp}\left(q^2\xi_\perp + \Omega_\perp\right) \end{pmatrix}. \tag{6}$$

Relativistic symmetry of the holographic setup enforces that the momentum and energy current densities must be equal $\pi = j_e$, which places constraints on the transport coefficients:

$$\alpha_o = -\frac{\mu}{T}\sigma_o\,, \quad \bar\kappa_o = \frac{\mu^2}{T}\sigma_o\,, \quad \gamma_2 = -\frac{\mu}{T}\gamma_1\,. \tag{7}$$

Observe that this also means that the heat current $j_q \equiv j_e - \mu j = \pi - \mu j$. Finally, the susceptibility matrix is[1]

$$\chi_{AB} = \begin{pmatrix} \chi_{\rho\rho} & \chi_{\rho s} & 0 & 0 & 0 & 0 \\ \chi_{\rho s} & \chi_{ss} & 0 & 0 & 0 & 0 \\ 0 & 0 & \chi_{\pi\pi} & 0 & 0 & 0 \\ 0 & 0 & 0 & \frac{q^2}{Kq^2 + G(q^2+m^2)} & 0 & 0 \\ 0 & 0 & 0 & 0 & \chi_{\pi\pi} & 0 \\ 0 & 0 & 0 & 0 & 0 & \frac{q^2}{G(q^2+m^2)} \end{pmatrix}. \tag{8}$$

A nonzero Goldstone mass implies that the Goldstone static susceptibilities $\chi_{\varphi_i\varphi_j}$ are finite in the limit $q \to 0$ (rather than divergent like $1/q^2$ if $m = 0$): there is no long range translational order in the system in the presence of explicit breaking.

[1] In general, nonzero static susceptibilities $\chi_{\rho\lambda_\parallel}$, $\chi_{s\lambda_\parallel}$ are also allowed. They play no role in our analysis, so we have set them to zero.

Positivity of entropy production can be ensured by requiring all the eigenvalues of the matrix M to be positive [2]. This implies:

$$\eta \geq 0, \qquad \sigma_o \geq 0\,, \qquad \gamma_1^2 \leq \sigma_o \frac{\xi_\parallel}{K+G}\,. \tag{9}$$

Using (5) and identities between the Green's functions stemming from (3) gives the retarded Green's functions quoted in equation (3) of the main text (with relaxation parameters turned off). We defined *eg*

$$G^R_{\varphi_i\varphi_j} = \frac{q_i q_j}{q^4} G^R_{\lambda_\parallel\lambda_\parallel} + \left[\delta_{ij} - \frac{q_i q_j}{q^2}\right] \frac{G^R_{\lambda_\perp\lambda_\perp}}{q^2}\,. \tag{10}$$

In this $q = 0$ limit, and in absence of relaxation, for an isotropic crystal, $G^R_{\lambda_\parallel\lambda_\parallel} = G^R_{\lambda_\perp\lambda_\perp}$, since there should be no distinction between the longitudinal and transverse phonons. This leads to the constraint

$$\frac{\xi_\parallel}{K+G} = \frac{\xi_\perp}{G} \equiv \Xi\,. \tag{11}$$

Of direct interest to us is the presence in the longitudinal part of the spectrum of a diffusive mode, which in the limit of small bulk and shear moduli takes the simple expression:

$$\omega = -i\xi_\parallel q^2 + O(K,G) + O(q^4)\,. \tag{12}$$

This diffusive mode can be thought of as encoding the dissipation of the longitudinal Goldstone mode at long distances.

When translations are broken explicitly but the breaking is weak, the two Goldstone damping rates $\Omega_\parallel$, $\Omega_\perp$ become q-dependent (see [2]). In the long distance limit applicable to conductivities, $q \ll m$, they are equal $\Omega_\parallel = \Omega_\perp \equiv \Omega$. Although explicit translation symmetry breaking was not considered as a microscopic origin for Ω in [2], the functional form of the hydrodynamic equations and retarded Green's functions is insensitive to the microscopic origin of such terms. Phonon damping by disorder was studied very early on, see eg [6, 7], but was reported to affect the ac conductivity only through a pinning mass m and momentum relaxation rate Γ [8]. Here we show that it also leads to phase relaxation Ω in the sense of [2, 9] and a nonzero dc conductivity. This is well-known from studies of the magnetic field-induced melting of Wigner solids [10, 11]

The conductivity equation (5) quoted in the Main text is defined from the retarded Green's function of the current

$$\sigma(\omega) \equiv \frac{i}{\omega} G^R_{jj}(\omega, q=0)\,. \tag{13}$$

The poles in the denominator of this expression are given in equation (6) of the main text, with the pinning frequency defined as $\omega_o^2 = Gm^2/\chi_{\pi\pi}$ and setting $\Gamma = 0$. For reference, we quote here its full expression without neglecting terms proportional to the momentum relaxation rate Γ:

$$\sigma(\omega) = \sigma_o + \frac{\frac{\rho^2}{\chi_{\pi\pi}}(\Omega - i\omega) - \omega_o^2\gamma_1\left[2\rho + \gamma_1\chi_{\pi\pi}\left(\Gamma - i\omega\right)\right]}{(\Gamma - i\omega)(\Omega - i\omega) + \omega_o^2}\,. \tag{14}$$

The Drude formula in equation (11) of the main text is recovered by setting the pinning frequency to zero or equivalently sending $\Omega \to +\infty$.

NUMERICAL METHODS

We have computed numerically black hole solutions to the action

$$S = \int d^4x\,\sqrt{-g}\left[R - \frac{1}{2}\partial\phi^2 - V(\phi) - \frac{1}{4}Z(\phi)F^2 - \frac{1}{2}\sum_{I=1}^{2}Y(\phi)\partial\psi_I^2\right]\,. \tag{15}$$

We adopt the following Ansatz for the metric and matter fields

$$ds^2 = \frac{1}{r^2}\left(-u(r)dt^2 + \frac{1}{u(r)}dr^2 + c(r)(dx^2 + dy^2)\right)\,, \tag{16}$$

$$A = A_t(r)dt\,, \quad \phi = \phi(r)\,, \quad \psi_I = kx^I\,, \quad x^I = \{x, y\}\,, \tag{17}$$

which allows for solutions that break translations pseudo-spontaneously. This follows from the Ansatz for the scalars ψ_I and the asymptotic behavior of the scalar coupling $Y(\phi)$, as explained in the Main text.

The resulting equations of motion can be reduced to a system of four ordinary differential equations (three are second order and one is first order). The scalar couplings behave in the UV as

$$V_{uv}(\phi) = -6 - \phi^2 + O(\phi^3), \quad Z_{uv}(\phi) = 1 + O(\phi), \quad Y_{uv}(\phi) = \phi^2 + O(\phi^3)\,. \tag{18}$$

The asymptotic behavior of the metric and matter fields is

$$\phi(r) = \lambda\, r + v\, r^2 + \frac{1}{36c_0^2}\left[-9c_1\left(c_1\,\lambda + 4c_0\,v\right) + c_0\,\lambda\left(36k^2 + 7c_0\,\lambda^2\right)\right]\, r^3 + O(r^4)\,, \tag{19a}$$

$$A_t(r) = \mu - \rho\, r + O(r^2)\,, \tag{19b}$$

$$u(r) = 1 + \frac{c_1}{c_0}\, r + \frac{1}{4}\left(\frac{c_1^2}{c_0^2} - \lambda^2\right) r^2 + u_3\, r^3 + O(r^4)\,, \tag{19c}$$

$$c(r) = c_0 + c_1\, r + \frac{1}{4c_0}\,\left(c_1^2 - c_0^2\,\lambda^2\right) r^2 - \frac{\lambda}{6}\left(c_1\,\lambda + 2c_0\,v\right) r^3 + O(r^4)\,, \tag{19d}$$

where higher order coefficients are functions of λ, v, ρ, u_3, c_0, and c_1. Notice that in order for this solution to asymptote to AdS we must have $c_0 = 1$, and $c_1 = 0$. ρ is the charge density, μ the chemical potential and v is related to the vev of the scalar ϕ.

We can also expand the solution near the black hole horizon $r = r_h$:

$$\phi(r) = \phi_h + O(r_h - r)\,, \qquad A_t(r) = A_{h,1}(r_h - r) + O((r_h - r)^2)\,, \tag{20a}$$

$$u(r) = u_{h,1}(r_h - r) + O((r_h - r)^3)\,, \quad c(r) = c_h + c_{h,1}(r_h - r) + O((r_h - r)^2)\,. \tag{20b}$$

In our numerics, we choose for the potentials

$$V(\phi) = -6\cosh(\phi/\sqrt{3}), \quad Z(\phi) = \exp(-\phi/\sqrt{3}), \quad Y(\phi) = (1 - \exp\phi)^2\,. \tag{21}$$

Then

$$u_{h,1} = \frac{c_h\, e^{-\frac{\phi_h}{\sqrt{3}}}\left[6 + e^{\frac{2\phi_h}{\sqrt{3}}}(6 - r_h^4\, A_{h,1})\right] - 2k^2 r_h^2\left(1 - e^{\phi_h}\right)^2}{2r_h\,(2c_h + c_{h,1}\, r_h)} \tag{22}$$

determines the temperature of the black hole $T = -u_{h,1}/(4\pi)$, and further higher order coefficients in (20) are also determined in terms of ϕ_h, $A_{h,1}$, c_h, and $c_{h,1}$.

By using the scale invariance $(t, x, y, r) \to \alpha\,(t, x, y, r)$, $A_t \to A_t/\alpha$, $k \to k/\alpha$ of the equations of motion, we can set the horizon radius $r_h = 1$ in our numerical computations. Numerical solutions are generated by integrating the equations of motion from the IR ($r = 1$) to the UV ($r = 0$). Using another scale invariance of the equations under $(x, y) \to \beta\,(x, y)$, $k \to k/\beta$, $c \to c/\beta^2$, we set $c_0 = 1$ This fixes c_h, leaving three free IR parameters ϕ_h, $A_{h,1}$, $c_{h,1}$; and one UV condition: $c_1 = 0$. Therefore, for each value of k we expect to obtain a two-parameter family of solutions. We can choose those parameters to be the dimensionless ratios T/μ, λ/μ. All in all we can parametrize the space of solutions in terms of the three dimensionless ratios T/μ, λ/μ, and k/μ.

In this work we are interested in solutions breaking translations pseudo-spontaneously. These are geometries where $\lambda/\mu \ll v/\mu^2$.

Low temperature, near horizon geometry

As we decrease the temperature below $T_{\rm qc} \simeq 5.10^{-2}\mu$, the scalar ϕ diverges near the horizon. The scalar couplings become

$$V_{IR} = -3e^{-\phi/\sqrt{3}}\,, \quad Z_{IR} = e^{-\phi/\sqrt{3}}\,, \quad Y_{IR} = 1\,, \tag{23}$$

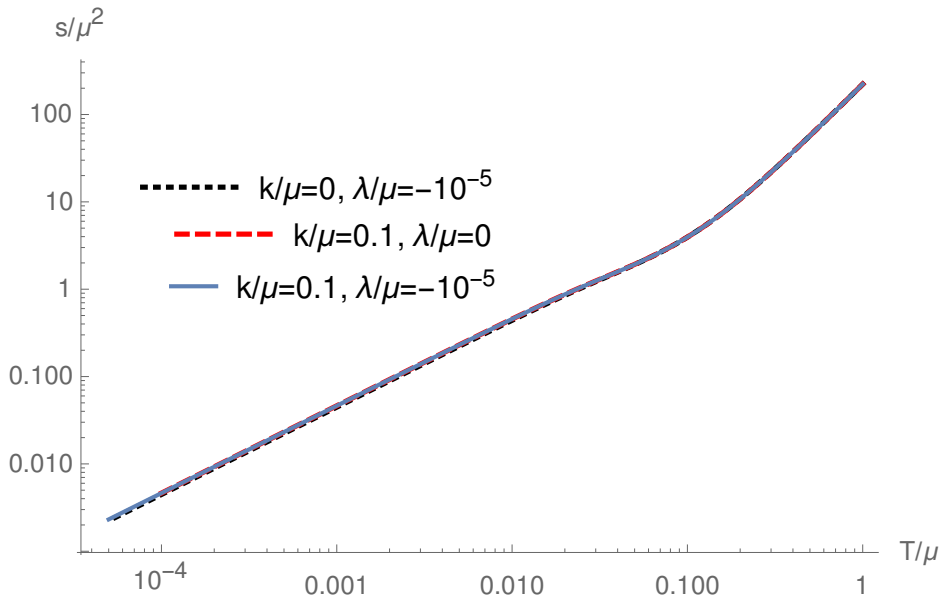

FIG. 1. Comparison of the entropy density vs temperature for various values of k and λ.

leading to a solution of the equations of motion conformal to $\mathrm{AdS}_2 \times R^2$, with a dynamical Lifshitz exponent $z = +\infty$ [12–16]:

$$\begin{aligned} ds^2 &= \frac{1}{\xi}\left[-\frac{f(\xi)}{\xi^2}L_t^2 dt^2 + \frac{\tilde{L}^2 d\xi^2}{\xi^2 f(\xi)} + L_x^2 dx^2 + L_x^2 dy^2\right], \quad A = a_o\,\xi^{-2} dt\,, \\ \phi &= -\sqrt{3}\log\xi\,, \quad f(\xi) = 1 - \left(\frac{\xi}{\xi_h}\right)^2. \end{aligned} \tag{24}$$

This solution is valid for values of the IR radial coordinate $\xi \gg \mu$. The constants L_t, L_x, $\tilde{L}$, a_o can be determined by matching to the UV AdS_4 asymptotics. In these coordinates, $T \sim \xi_h^{-1}$, so that the entropy density $s \sim \xi_h^{-1} \sim T$.

A rough estimate of the temperature T_{qc} where the near horizon geometry becomes conformal to $\mathrm{AdS}_2 \times R^2$ is given by the temperature below which the entropy density becomes linear in temperature. This is displayed in figure 1 for various values of k and λ. All curves fall on top of one another, which demonstrates that T_{qc} is relatively insensitive to the specific value of k and λ for the typical ranges we are interested in.

AC Correlators: Conductivity and QNMs

In order to compute the conductivity of the boundary theory and the QNMs at zero momentum, it is sufficient to study the following consistent set of fluctuations

$$\delta g_{tx} = h(r)\, e^{-i\omega t}\,, \quad \delta A_x = a(r)\, e^{-i\omega t}\,, \quad \delta\psi_x = \xi(r)\, e^{-i\omega t}\,. \tag{25}$$

To linear order in the fluctuations, the equations of motion for a, h, and ξ are a consistent set formed by two second order and one first order differential equation.

For a pseudo-spontaneous background geometry with $\lambda \neq 0$, the fluctuations have the following UV expansion

$$h(r) = r^{-2}\left(h_0 + O(r^3)\right)\,, \tag{26a}$$

$$a(r) = a_0 + a_1\, r + O(r^2)\,, \tag{26b}$$

$$\xi(r) = \xi_0 + \xi_1 r + O(r)\,, \tag{26c}$$

where higher order coefficients are functions of h_0, a_0, a_1, ξ_1 and ξ_0.

The AC conductivity can be read from $G^R_{j^x j^x}$ through a Kubo formula which in terms of the asymptotic expansion (26) takes the form

$$\sigma(\omega) = \frac{1}{i\omega}\, G^R_{j^x j^x}(\omega) = \frac{a_1}{i\omega\, a_0}\,. \tag{27}$$

The second equality holds for configurations where the only nonzero source is given by a_0 which corresponds to turning on an electric field along x. The only other independent source in the UV solution (26) is given by the diffeomorphism-invariant combination

$$\xi_0 - \frac{ik}{\omega}\, h_0\,, \tag{28}$$

and it should vanish on the solutions used to compute $\sigma(\omega)$ through (27).

We are interested in computing a retarded correlator, hence we look for solutions with ingoing boundary conditions at the black hole horizon. They read

$$h(r)\, e^{i\frac{\omega}{u_{h,1}}} = h_{h,1}\,(r_h - r) + O((r_h - r)^2)\,, \tag{29a}$$

$$a(r)\, e^{i\frac{\omega}{u_{h,1}}} = a_h + O(r_h - r)\,, \tag{29b}$$

$$\xi(r)\, e^{i\frac{\omega}{u_{h,1}}} = \xi_h + O(r_h - r)\,, \tag{29c}$$

with

$$h_{h,1} = \frac{a_h\, A_{h,1}\, e^{-\frac{\phi_h}{\sqrt{3}}}\, r_h^2 - \left(e^{\phi_h}-1\right)^2 \xi_h\, k/r_h}{i\omega/u_{h,1} - 1}\,, \tag{30}$$

and other higher order coefficients determined as well in terms of a_h, and ξ_h.

We construct numerical solutions by integrating the system of three linear differential equations for h, a, ξ from the horizon ($r = r_h = 1$) to the boundary ($r = 0$). There are two free IR parameters in (29), but since the equations are linear we can scale away one of them (eg set $a_h = 1$). Therefore we are left with one free (complex) parameter and one UV boundary condition: we shoot for solutions where the combination (28) vanishes, and read $\sigma(\omega)$ using (27).

We shall next compute the QNMs given by the poles of the holographic correlator $G^R_{AB}(\omega)$ where $A, B = h, a, \xi$ are the set of fields (25). We follow [17] and employ the so-called determinant method. Hence we need to obtain three independent solutions for the fluctuations, and construct the following matrix of sources

$$S = \begin{pmatrix} h_0^{(I)} & h_0^{(II)} & -i\omega \\ a_0^{(I)} & a_0^{(II)} & 0 \\ \xi_{-1}^{(I)} & \xi_{-1}^{(II)} & k \end{pmatrix}\,, \tag{31}$$

where in order to generate the third column we have used the pure gauge solution

$$h(r) = -i\omega\, \frac{c(r)}{r^2}\,, \quad a(r) = 0\,, \quad \xi(r) = k\,. \tag{32}$$

It is straightforward to construct two independent numerical solutions integrating from the horizon with boundary conditions (29).

Finally, the QNMs, namely the complex frequencies where the holographic Green functions have a pole, are given by the values of ω for which the determinant of the matrix (31) vanishes [17].

ψ CORRELATORS AT $k = 0$

In this appendix, we solve the equations of motion and compute the correlators of the fields ψ_I in the limit $k = 0$. Similar results have also been reported in [18]. In this case, both fields decouple and so we will just denote them by $\delta\psi$. The equation of motion for the

fluctuation $\delta\psi = \delta\psi(r)\exp(-i\omega t + iqx)$ is

$$\left(\sqrt{\frac{D}{B}}CY\delta\psi'\right)' + \left(\omega^2 - \frac{D}{C}q^2\right)CY\sqrt{\frac{B}{D}}\delta\psi = 0\,. \tag{33}$$

Using a standard procedure in holography [19–21], this equation can be solved perturbatively at small ω, q compared to r_h, assuming the presence of a regular black hole horizon. We consider the expansion of the perturbation

$$\delta\psi(r) = \left(1 - \frac{r}{r_h}\right)^{-\frac{i\omega}{4\pi T}}\left(1 + \frac{i\omega}{4\pi T}\delta\psi_1 + \left(\frac{q}{4\pi T}\right)^2\delta\psi_2 + O\left(q^3, \omega^3, \omega q^2\right)\right). \tag{34}$$

After transforming to Eddington-Finkelstein coordinates, this corresponds to the ingoing mode at the horizon [22]. The horizon is located at $r = r_h$ and the boundary at $r = 0$. Plugging (34) into (33), the equation is solved perturbatively order by order in ω.

The order ω^0 is trivially solved by a constant, which can always be set to unity by linearity of the equation of motion. The solution at $O(\omega)$ reads

$$\delta\psi_1(r) = \int_{r_h}^{r} dr\left(\frac{4\pi T C_h Y_h\sqrt{B}}{CY\sqrt{D}} - \frac{1}{r_h - r}\right), \tag{35}$$

where we have imposed horizon regularity to fix one of the integration constants, and chose the other one such that $\delta\psi_1(r_h) = 0$ (which otherwise would simply correspond to a different choice of normalization of the source).

The solution for $\delta\psi_2$ after imposing horizon regularity is

$$\delta\psi_2 = (4\pi T)^2\int_{r_h}^{r}\frac{\sqrt{B}}{\sqrt{D}CY}\int_{\tilde{r}_h}^{\tilde{r}}\sqrt{BD}Y\,. \tag{36}$$

We now put everything together back in (34) and expand close to the boundary. For nonzero source $\lambda \neq 0$, the asymptotic expansion of $\delta\psi$ takes the form

$$\delta\psi(r \to 0) = \delta\psi^{(0)} + r\delta\psi^{(1)} + \dots \tag{37}$$

where the r^0 term is the source and the r^1 term is related to the vev by

$$\langle O_{\delta\psi}\rangle = \lambda^2\delta\psi^{(1)}\,. \tag{38}$$

We find

$$G^R_{\delta\psi\delta\psi} = \frac{i\omega C_h Y_h - q^2 I_Y}{1 - i\omega\tau_o + \tau_o D_\psi q^2}\,, \tag{39}$$

with

$$\tau_o = \int_0^{r_h} dr \left(\frac{C_h Y_h \sqrt{B}}{CY\sqrt{D}} - \frac{1}{4\pi T} \frac{1}{r_h - r} \right), \tag{40}$$

and

$$D_\psi = \frac{1}{\tau_o} \int_{r_h}^{0} \frac{\sqrt{B}}{\sqrt{D} CY} \int_{r_h}^{\tilde{r}} \sqrt{BD} Y \,. \tag{41}$$

This gives a pseudo-diffusive pole located at

$$\omega_{k=0,\lambda\neq 0} = -i\Omega - iD_\psi q^2 + O(q^4)\,, \quad \Omega = \frac{1}{\tau_o}\,, \tag{42}$$

which matches very well the exact location of the pole determined numerically, see figures 2 and 3. The exact numerical dispersion relation deviates from (42) as q increases or as T decreases, which is expected. Actually, at sufficiently low T or large q, the pole collides with another purely imaginary pole and moves off axis. This collision and subsequent motion of the poles matches very well the motion of the two CM poles in figure 1 of the main text at the lowest temperatures $T < T_{\rm cm}$.

In figure 4, we compare the collision temperature $T_{\rm cm}$ at $k = 0$ and $k/\mu = 0.1$ by plotting the real part of the relevant QNMs close to the collision. At $\lambda/\mu = -10^{-5}$, there is little variation between $k = 0$ and $k/\mu = 0.1$. On the other hand, varying λ/μ from -10^{-5} to -5.10^{-7} shows that $T_{\rm cm}$ depends in a much more pronounced way on the value of λ, which is expected since $\tau_o^{-1} \sim \lambda$ (see top row of figure 7 below). Indeed, $T_{\rm cm} = 0$ in the purely spontaneous limit $\lambda = 0$, [23].

The presence of an overdamped mode when $\lambda \neq 0$ is a consequence of the explicit breaking of the global shift symmetry $\psi \mapsto \psi + c$. It is easy to check that when $\lambda = 0$, the gap vanishes and the mode (42) becomes purely diffusive

$$\omega_{k=0,\lambda=0} = -i\xi q^2\,, \qquad \xi \equiv \frac{I_Y}{C_h Y_h} \tag{43}$$

which coincides with the $k \to 0$ limit of the CM diffusivity $G\Xi$ in equation (6) of the main text. Turning λ back on, we expect that

$$D_\psi = \xi + O(\lambda) = \frac{I_Y}{C_h Y_h} + O(\lambda)\,, \tag{44}$$

which we verify numerically in figure 5. Small deviations appear at very low temperature, upon approaching the pole collision. This is because the corrections of $O(\lambda)$ are no longer small compared to T.

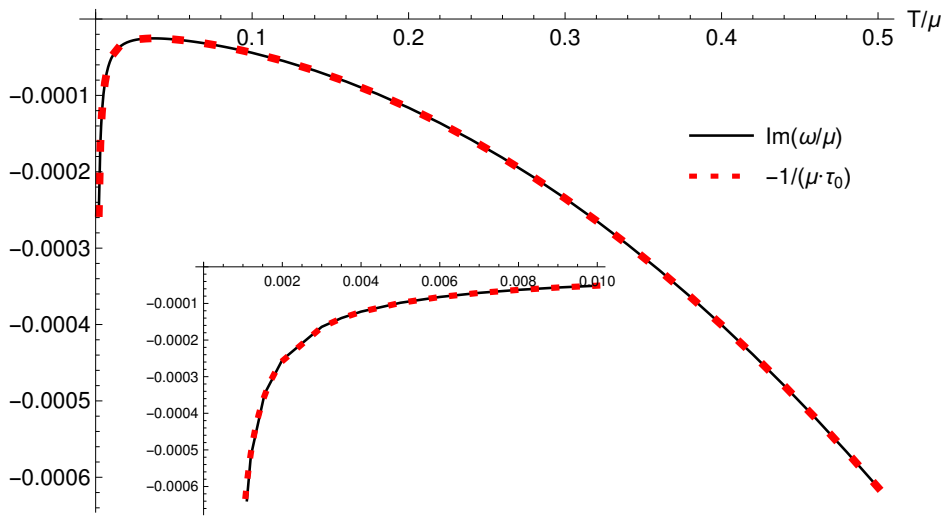

FIG. 2. Numerical check that the gap in (42) at $q = 0$ is well-captured by (40). Data for $\lambda/\mu = -10^{-5}$.

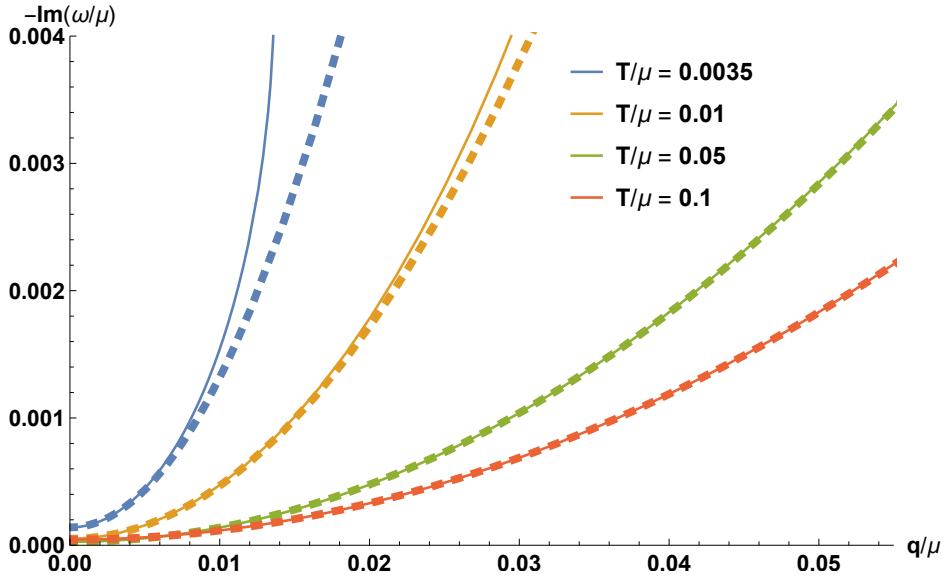

FIG. 3. Numerical check of the dispersion relation (42). Solid lines represent the numerical data and dashed lines correspond to equation (42).

Holographic and hydrodynamic correlators may differ by contact terms [5], so we compare

$$G^R_{\varphi_\perp\varphi_\perp}(\omega,q) - G^R_{\varphi_\perp\varphi_\perp}(\omega=0,q) = \frac{1}{G}\frac{i\omega}{(q^2+m^2)(i\omega-\Omega-q^2\xi)} + O(G^0,\Gamma^0\sim k^0) \tag{45}$$

to

$$G^R_{\delta\psi\delta\psi}(\omega,q) - G^R_{\delta\psi\delta\psi}(\omega=0,q) = -\frac{i\omega\Omega\left(C_h Y_h \Omega + q^2(C_h Y_h D_\psi - I_Y)\right)}{(D_\psi q^2+\Omega)\left(i\omega-\Omega-D_\psi q^2\right)}\,. \tag{46}$$

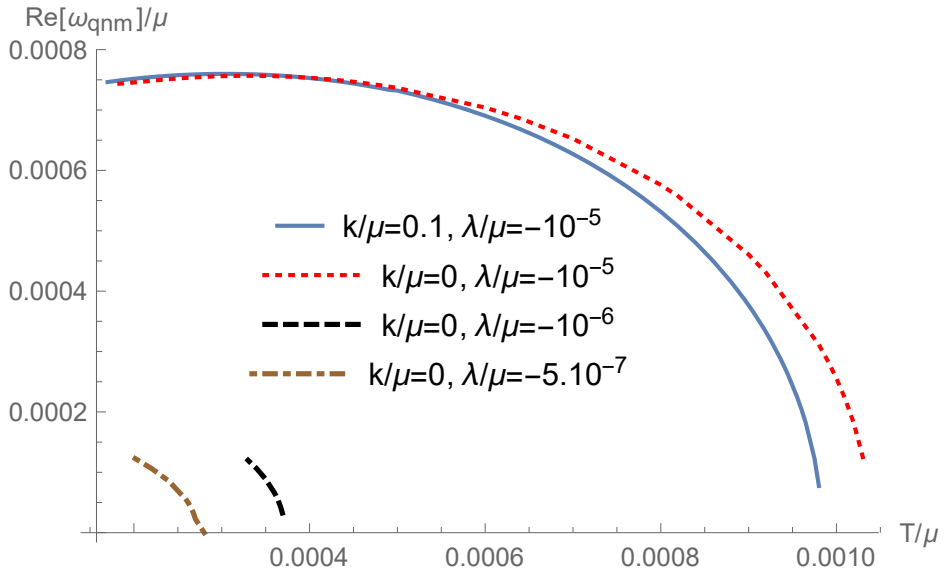

FIG. 4. Real part of the longest-lived complex QNMs at low temperatures $T \leq T_{\rm cm}$ ($T_{\rm cm}$ is the temperature at which the real part vanishes), showing the dependence of $T_{\rm cm}$ on k and λ.

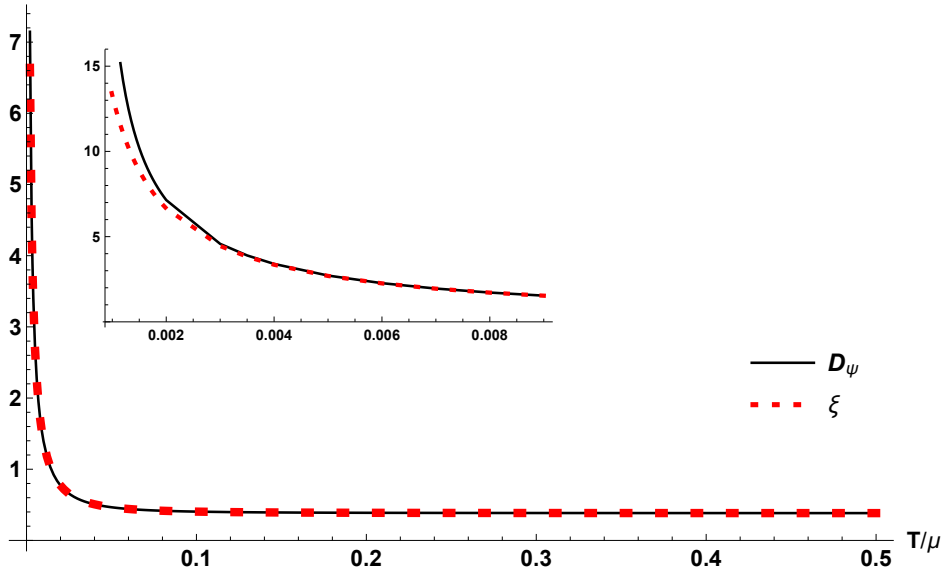

FIG. 5. Numerical check of equation (44).

The two expressions can be seen to match since from (44) $D_\psi \simeq \xi \simeq I_Y/(C_h Y_h)$ and $m^2 \simeq \Omega/\xi$, as we verify in figure 6, after identifying the boundary Goldstone mode and the vev of the bulk operator $\delta\psi$ as

$$\langle O_{\delta\psi} \rangle = \lambda^2 \delta\psi^{(1)} = \frac{G m^2}{k} \varphi \,. \tag{47}$$

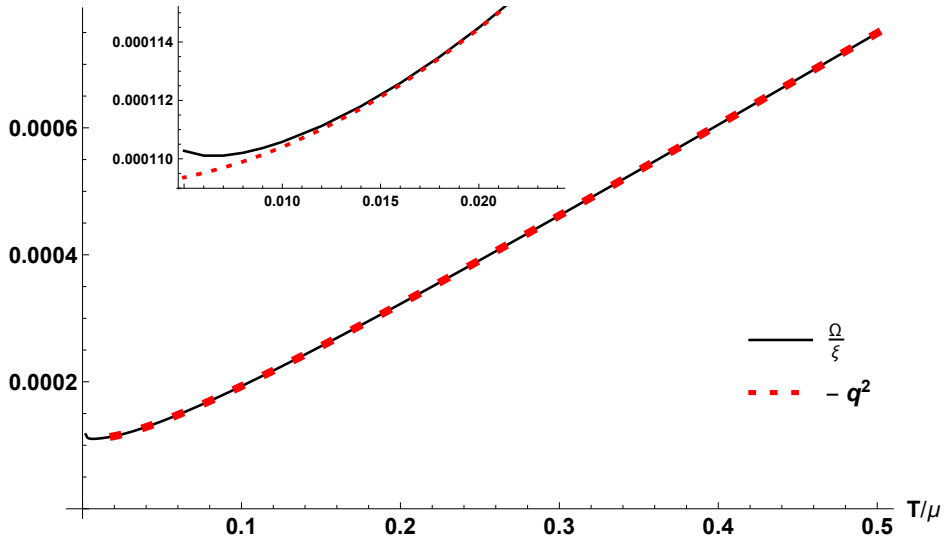

FIG. 6. Numerical check that there is a pole in (39) at $\omega = 0$, $q^2 = -m^2 \simeq -\Omega/\xi$.

λ AND k DEPENDENCE OF THE RELAXATION PARAMETERS

Using the quasi-normal modes computed numerically together with the hydrodynamic expression for the conductivity (14) and the analytic expression for the diffusivity γ_1 (formula (4) of the main text), we have been able to compute the relaxation parameters Ω, Γ and ω_o and to fit their k and λ dependence. The results are shown in figures 7, 8 and 9 for two different values of the temperature: the red dots refer to $T/\mu = 0.5$ and the blue dots to $T/\mu = 0.0035$.

The result of the fitting analysis is:

$$\Omega \sim |\lambda| k^0 \ , \qquad \Gamma \sim |\lambda| k^2 \ , \qquad \omega_o \sim |\lambda|^{1/2} k \ , \tag{48}$$

as reported in the main text. All our best fits include a small intercept, which is typically very close to our numerical zero and should be disregarded.

At either very small k or λ, the dc conductivity we use to extract the relaxation parameters becomes very large, and our numerical procedure loses accuracy. This is particularly apparent in the left panel of figure 9, which shows the dependence of Γ on k at high T. We find values of Γ/μ of order 10^{-12}, which we do not regard as very reliable. For all intents and purposes, Γ should be set to zero, which we have done in the main text. This is further justified by the fact that in this range of k, $\Gamma \ll \omega_o^2/\Omega$, as shown in the right plot in fig 9. Moreover, we have verified that the values of Ω and ω_o obtained setting $\Gamma = 0$ are quasi-identical to those obtained keeping $\Gamma \neq 0$. At fixed $\lambda/\mu = -10^{-5}$ and $T/\mu = 0.0035$, we

obtain values for Γ oscillating between tiny positive and negative values, once again with little effect on the values of Ω and ω_o. For this reason, we have set $\Gamma = 0$ for the results presented in the right column of figure 8. As a final check, we have verified that the $k \to 0$ limits for the parameters Ω and m agree with the values we find setting $k = 0$ exactly, as is done in the previous section.

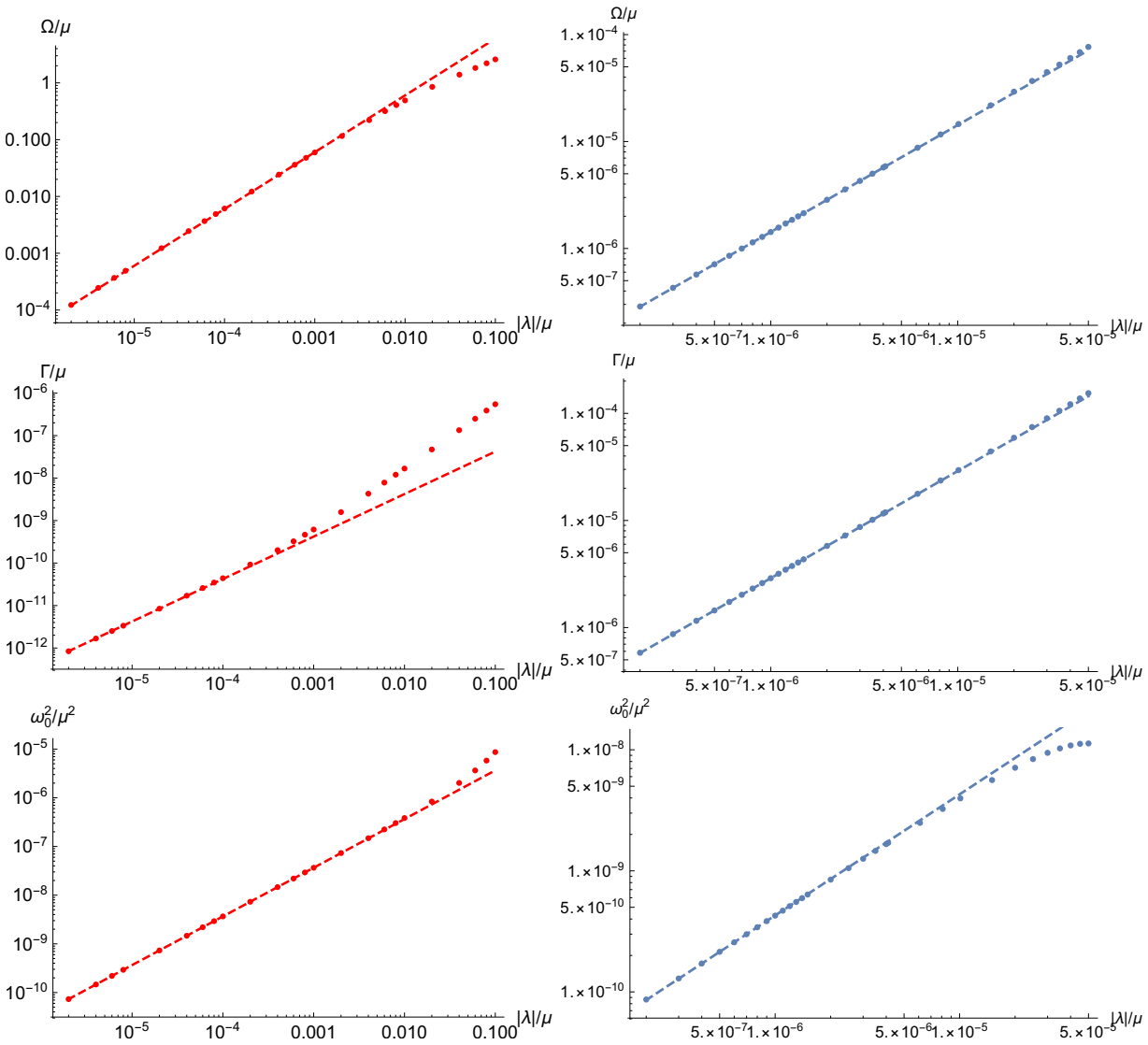

FIG. 7. Bi-log plots of the λ dependence of Ω, Γ and ω_o and their best fits (dashed lines) at $k/\mu = 0.1$, revealing the scalings reported in equation (48). The red dots are for $T/\mu = 0.5$ while the blue dots are for $T/\mu = 0.0035$.

Figure 10 shows the λ dependence of the ratio $\Gamma/(\omega_o^2/\Omega)$ at high and low temperature. As one can see from the plots, for small $|\lambda|/\mu$ (e.g. $\lambda/\mu = -10^{-5}$ as it is considered in the

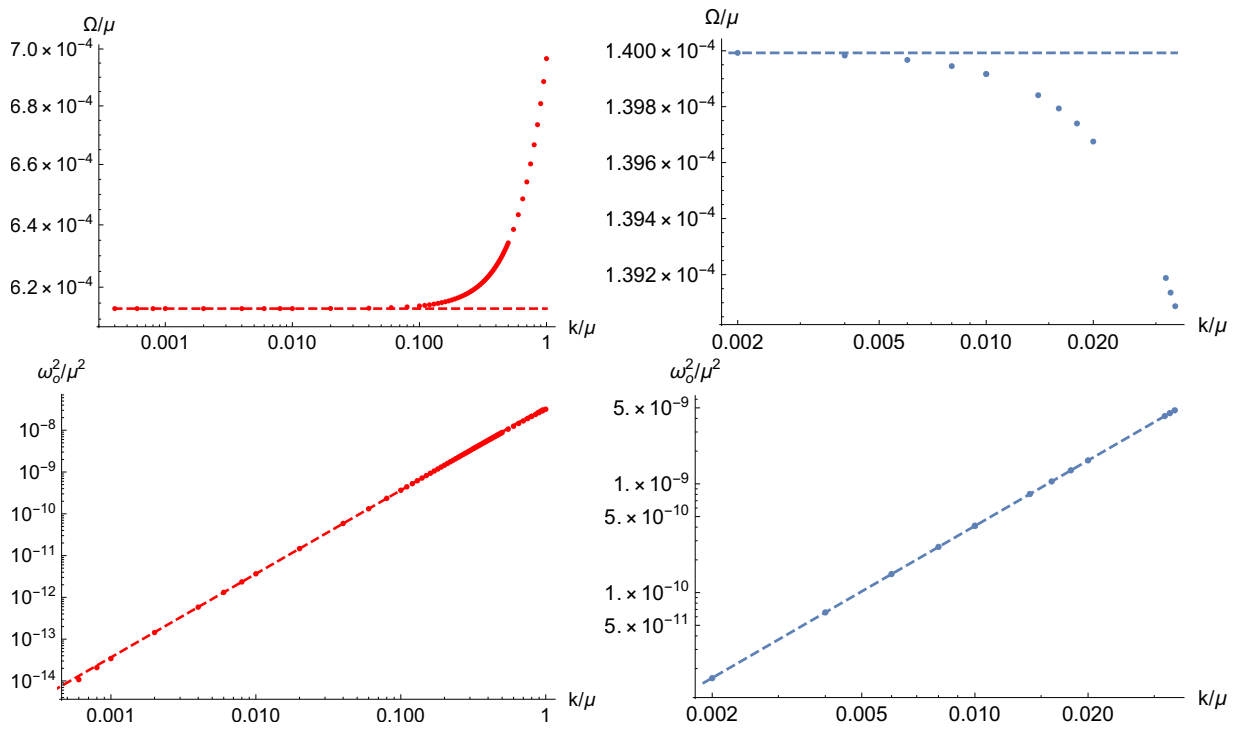

FIG. 8. Bi-log plots of the k dependence of Ω and ω_o and their best fits (dashed lines) for $\lambda/\mu = -10^{-5}$, revealing the scalings reported in equation (48). The red dots are for $T/\mu = 0.5$ while the blue dots are for $T/\mu = 0.0035$. As explained in the text, we have set $\Gamma = 0$ for $T/\mu = 0.0035$. For Ω (top row), the dashed line is a guide to the eye, from our lowest value of k available, in very good agreement with the value of Ω at $k = 0$ exactly.

main text) the ratio is very small with a very weak dependence on $|\lambda|/\mu$, implying that Γ can be safely neglected as is done in presenting the results in the main text. The situation is different increasing $|\lambda|/\mu$, since Γ becomes comparable to ω_o^2/Ω for large enough λ/μ. This is expected since by increasing λ/μ we are moving from the pseudo-spontaneous to the purely explicit regime, where any spontaneous component of the system is washed out and Γ is the dominant relaxation scale.

Figure 11 shows the λ dependence of the ratio $\Omega/(Gm^2\Xi)$ at high and low temperature. For small $|\lambda|$, the dependence on $|\lambda|$ is also very weak, before increasing more sharply as the explicit regime is approached.

Finally, we have checked that as k is varied from very low values up to values $k/\mu = 1$, the ratio $\Omega/(Gm^2\Xi)$ shows no significant deviations from unity.

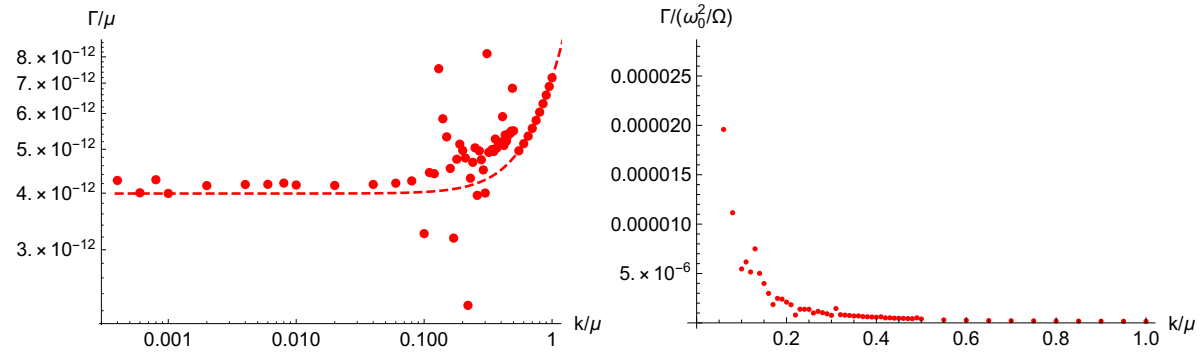

FIG. 9. Left: k dependence of Γ for $T/\mu = 0.5$ and $\lambda/\mu = -10^{-5}$, revealing the scaling reported in equation (48). Even though the data becomes noisy at low k, it is consistent with the best quadratic fit determined from the higher k data. The tiny value for the intercept is close to the machine precision and we regard it as a numerical zero. Right: k dependence of the ratio $\Gamma/(\omega_o^2/\Omega)$ for $T/\mu = 0.5$ and $\lambda/\mu = -10^{-5}$.

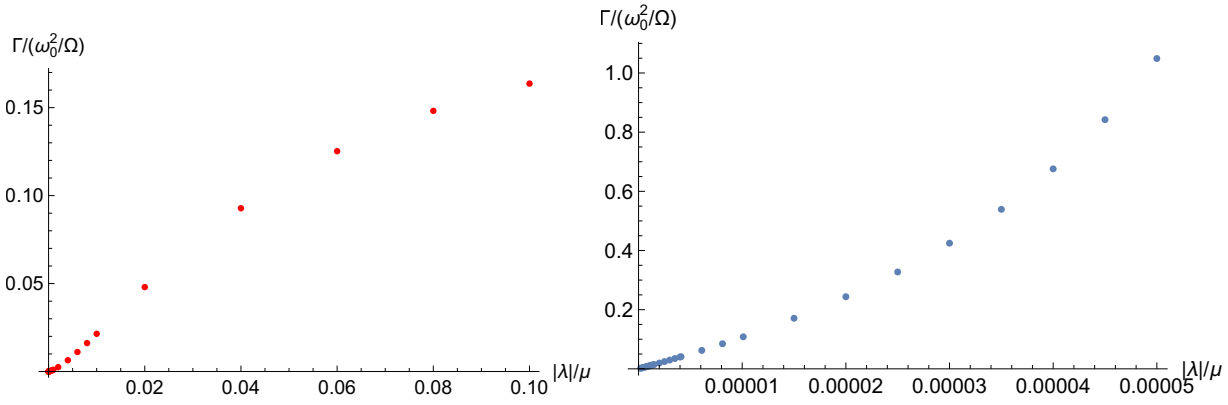

FIG. 10. λ dependence of the quantity $\Gamma/(\omega_o^2/\Omega)$ for $k/\mu = 0.1$. Left: $T/\mu = 0.5$. Right: $T/\mu = 0.0035$. For small enough $|\lambda|$, Γ can be neglected compared to ω_o^2/Ω.

We are grateful to Hyun-Sik Jeong and Keun-Young Kim for pointing out some typos in a previous version of this SM.

* andrea.amoretti@ge.infn.it

† daniel.arean@uam.es

‡ blaise.gouteraux@polytechnique.edu

§ daniele.musso@usc.es

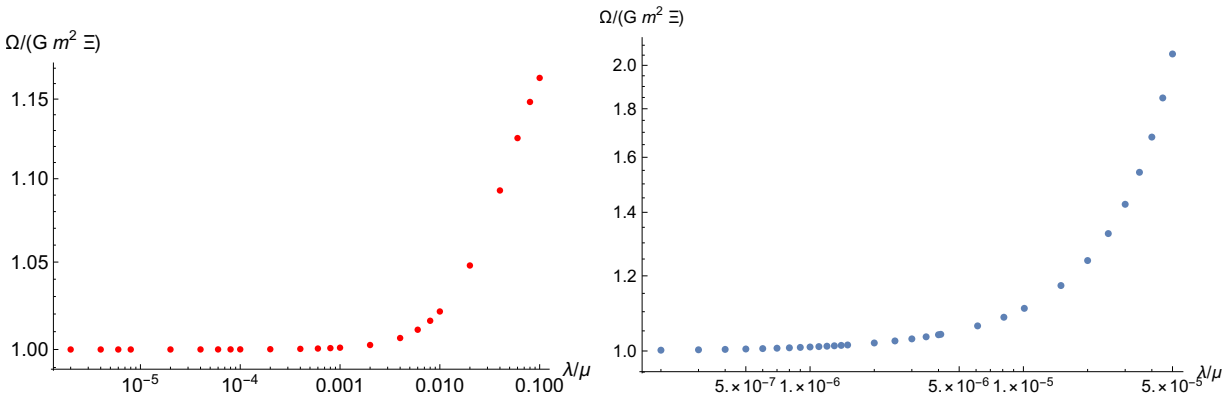

FIG. 11. λ dependence of the ratio $\Omega/(Gm^2\Xi)$ for $k/\mu = 0.1$. Left: $T/\mu = 0.5$. Right: $T/\mu = 0.0035$.

[1] P. M. Chaikin and T. C. Lubensky, *Principles of Condensed Matter Physics* (Cambridge University Press, 1995).

[2] Luca V. Delacrétaz, Blaise Goutéraux, Sean A. Hartnoll, and Anna Karlsson, "Theory of hydrodynamic transport in fluctuating electronic charge density wave states," Phys. Rev. **B96**, 195128 (2017), arXiv:1702.05104 [cond-mat.str-el].

[3] Aron J. Beekman, Jaakko Nissinen, Kai Wu, Ke Liu, Robert-Jan Slager, Zohar Nussinov, Vladimir Cvetkovic, and Jan Zaanen, "Dual gauge field theory of quantum liquid crystals in two dimensions," Phys. Rept. **683**, 1–110 (2017), arXiv:1603.04254 [cond-mat.str-el].

[4] Leo P Kadanoff and Paul C Martin, "Hydrodynamic equations and correlation functions," Annals of Physics **24**, 419 – 469 (1963).

[5] Pavel Kovtun, "Lectures on hydrodynamic fluctuations in relativistic theories," *INT Summer School on Applications of String Theory Seattle, Washington, USA, July 18-29, 2011*, J. Phys. **A45**, 473001 (2012), arXiv:1205.5040 [hep-th].

[6] H. Fukuyama and P. A. Lee, "Dynamics of the charge-density wave. i. impurity pinning in a single chain," Phys. Rev. B **17**, 535–541 (1978).

[7] W. Finger and T. M. Rice, "Long-wavelength phonons in incommensurate systems," Phys. Rev. B **28**, 340–358 (1983).

[8] G. Grüner, "The dynamics of charge-density waves," Rev. Mod. Phys. **60**, 1129–1181 (1988).

[9] Luca V. Delacrétaz, Blaise Goutéraux, Sean A. Hartnoll, and Anna Karlsson, "Bad Metals from Fluctuating Density Waves," SciPost Phys. **3**, 025 (2017), arXiv:1612.04381 [cond-

mat.str-el].

[10] Hidetoshi Fukuyama and Patrick A. Lee, "Pinning and conductivity of two-dimensional charge-density waves in magnetic fields," Phys. Rev. B **18**, 6245 (1978).

[11] Michael M. Fogler and David A. Huse, "Dynamical response of a pinned two-dimensional Wigner crystal," Phys. Rev. B **62**, 7553 (2000).

[12] Richard J. Anantua, Sean A. Hartnoll, Victoria L. Martin, and David M. Ramirez, "The Pauli exclusion principle at strong coupling: Holographic matter and momentum space," JHEP **03**, 104 (2013), arXiv:1210.1590 [hep-th].

[13] Richard A. Davison, Koenraad Schalm, and Jan Zaanen, "Holographic duality and the resistivity of strange metals," Phys. Rev. **B89**, 245116 (2014), arXiv:1311.2451 [hep-th].

[14] B. Goutéraux, "Charge transport in holography with momentum dissipation," JHEP **04**, 181 (2014), arXiv:1401.5436 [hep-th].

[15] Andrea Amoretti, Daniel Areán, Blaise Goutéraux, and Daniele Musso, "Effective holographic theory of charge density waves," Phys. Rev. **D97**, 086017 (2018), arXiv:1711.06610 [hep-th].

[16] Andrea Amoretti, Daniel Areán, Blaise Goutéraux, and Daniele Musso, "DC resistivity of quantum critical, charge density wave states from gauge-gravity duality," Phys. Rev. Lett. **120**, 171603 (2018), arXiv:1712.07994 [hep-th].

[17] Matthias Kaminski, Karl Landsteiner, Javier Mas, Jonathan P. Shock, and Javier Tarrio, "Holographic Operator Mixing and Quasinormal Modes on the Brane," JHEP **02**, 021 (2010), arXiv:0911.3610 [hep-th].

[18] Aristomenis Donos, Daniel Martin, Christiana Pantelidou, and Vaios Ziogas, "Hydrodynamics of broken global symmetries in the bulk," (2019), arXiv:1905.00398 [hep-th].

[19] Giuseppe Policastro, Dam T. Son, and Andrei O. Starinets, "From AdS / CFT correspondence to hydrodynamics," JHEP **09**, 043 (2002), arXiv:hep-th/0205052 [hep-th].

[20] Giuseppe Policastro, Dam T. Son, and Andrei O. Starinets, "From AdS / CFT correspondence to hydrodynamics. 2. Sound waves," JHEP **12**, 054 (2002), arXiv:hep-th/0210220 [hep-th].

[21] Christopher P. Herzog, "The Sound of M theory," Phys. Rev. **D68**, 024013 (2003), arXiv:hep-th/0302086 [hep-th].

[22] Dam T. Son and Andrei O. Starinets, "Minkowski space correlators in AdS / CFT correspondence: Recipe and applications," JHEP **09**, 042 (2002), arXiv:hep-th/0205051 [hep-th].

[23] Andrea Amoretti, Daniel Areán, Blaise Goutéraux, and Daniele Musso, "Diffusion and uni-

versal relaxation of holographic phonons," (2019), arXiv:1904.11445 [hep-th].